

EFFICIENT IMPEDANCE COMPUTATION FOR MULTI-CONDUCTOR TRANSMISSION LINES OF RECTANGULAR CROSS SECTION

M. Matsuki and A. Matsushima*

Graduate School of Science and Technology, Kumamoto University,
2-39-1 Kurokami, Kumamoto 860-8555, Japan

Abstract—An efficient numerical solution is presented for computing per-unit-length impedance of metallic rectangular transmission lines backed by semi-infinite lossy substrate. We formulate the problem into the set of integral equations, the kernel of which is analytically expressed in terms of special functions in the quasi-static regime. The method of moments is applied to find the current density distributions in the metal regions, where the discretization of cross sections is performed by using non-uniform grid arranged according to the skin effect. The practical numerical computations concern the influence of the substrate loss on the per-unit-length impedance for some types of parallel lines. We thereby show that the substrate loss cannot be neglected at high frequencies. The effectiveness of the proposed method is confirmed by showing that the computed values of resistance satisfy the law of energy conservation with acceptable accuracy.

1. INTRODUCTION

With a recent rise in the clock frequency and integration density of VLSI, it has become necessary to estimate the per-unit-length resistance and inductance of interconnect accurately in order to maintain the signal and power integrity [1,2]. Success in efficient designs of transmission lines depends on how correctly the selected formulas or numerical methods can take into account the skin and proximity effects [3–5]. Toward this, much effort has been devoted to developing numerical techniques based on computational electromagnetics. The integral equation method, among others, is a powerful tool for finding per-unit length impedance or current density

Received 11 July 2012, Accepted 6 September 2012, Scheduled 13 September 2012

* Corresponding author: Akira Matsushima (matsua@cs.kumamoto-u.ac.jp).

distributions in the rectangular cross section of metallic lines [6–9]. In these works, however, the treated geometries are limited to the cases where the line conductors are free-standing or backed by lossless dielectric substrate. Considering that the increase in resistance due to the eddy current flowing in lossy semiconductor substrate has been raised many researchers' attention nowadays [10–12], it is advantageous if we can extend the powerful integral equation solutions to this case.

In view of the above, the present authors recently proposed an efficient numerical method for computing per-unit-length impedances of a free-standing single conductor line having rectangular cross section [13]. In the process of the moment method [14], discretization of the cross section was performed according to the skin effect by using nonuniform grid, which remarkably saves the computational cost. As a straightforward extension of the procedure in [13], the present paper deals with more practical structures, i.e., the multiconductor transmission lines backed by a substrate. With retaining the merit of this solution, we will extend the geometry of the line with regard to the number of conductors and the existence of lossy semi-infinite substrate. The effect of the substrate is taken into account in terms of a correction to the kernel function of the logarithmic type. The Sommerfeld integral can be analytically evaluated via the Struve and Neumann functions in the quasi-static regime.

The numerical computations are carried out for some types of parallel lines, composed of two, three, and four rectangular conductors, both with and without a substrate. Detailed investigation is made for the dependence of the per-unit-length impedance on the line parameters, such as size of the conductors, distance between them, conductance of the substrate, and thickness of the buffer layer. As a means of demonstrating the validity of the present solution, we mention the satisfaction of the law of energy conservation. This law states that the *total* resistance of the model is a sum of the *internal* and *external* ones, the latter of which stems from the eddy current loss. These three kinds of resistance are calculated based on the independent formulations. It is shown that the relative error on this law is always less than 1%.

2. NUMERICAL METHOD

2.1. Geometry of the Problem

As shown in Fig. 1, multiconductor transmission lines with rectangular cross section are arranged in parallel above the lossy substrate or perfectly conducting ground material. The cross section of the p -th line ($p = 1, 2, \dots, P$) is expressed as $S_p = \{\mathbf{r}(= \mathbf{i}_x x + \mathbf{i}_y y) | 0 <$

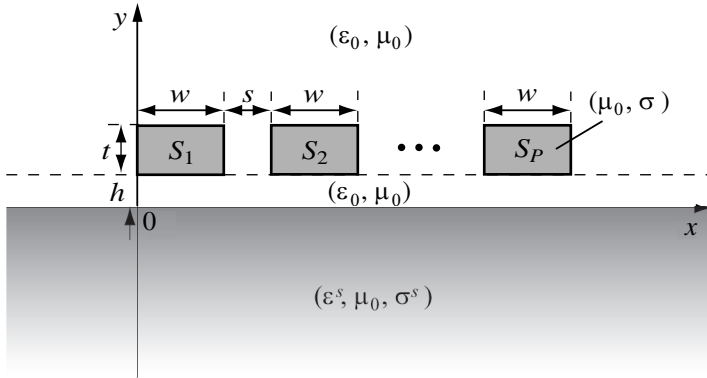


Figure 1. Multiconductor lines and semi-infinite substrate.

$x - (p - 1)(w + s) < w, 0 < y - h < t\}$, where \mathbf{i}_x and \mathbf{i}_y are the unit vectors in each direction. The lines are metallic with the permittivity ε^m and the conductivity σ . Nevertheless, ε^m will never appear in the analysis hereafter because the displacement current may be neglected compared with the conducting one. In fact, the ratio of the former to the latter is $\omega\varepsilon^m/\sigma \approx 5 \times 10^{-5} \ll 1$ (ω : angular frequency of the time-harmonic fields) in the worst-case estimate that $f = \omega/(2\pi) = 1$ THz, $\varepsilon^m = 10\varepsilon_0$, and $\sigma = 10^7$ S/m. The permittivity and conductivity of the substrate or ground region $y < 0$ are ε^s and σ^s , respectively. The permeability is assumed to be μ_0 everywhere. It is permissible to let the permittivity in the spacer layer $0 < x < h$ be equal to that in the vacuum, seeing that we will deal with only the magnetic field in it. Numbering of the lines, which is now sequential from left to right in Fig. 1, may be changed according to the choice of a reference conductor.

2.2. Vector Potential

Suppose that the current density $\mathbf{J}(\mathbf{r})$ in the lines has only the axial component $J_z(\mathbf{r})$. Then the vector potential $\mathbf{A}(\mathbf{r})$ has the same component, and it satisfies the Helmholtz equation

$$\left[\frac{\partial^2}{\partial x^2} + \frac{\partial^2}{\partial y^2} + \begin{pmatrix} \beta_0^2 \\ \beta^2 \end{pmatrix} \right] A_z(x, y) = 0 \quad \begin{pmatrix} y > 0 \\ y < 0 \end{pmatrix} \quad (1)$$

where $\beta_0^2 = \omega^2\varepsilon_0\mu_0$, $\beta^2 = \omega^2(\varepsilon^s - j\sigma^s/\omega)\mu_0$, and j is the imaginary unit with respect to time. The solution of (1) satisfying the continuity of A_z and $(\nabla \times \mathbf{A})_{x,y}$ at $y = 0$ is written in terms of the Fourier cosine

transform as

$$A_z(\mathbf{r}) = \frac{\mu_0}{\pi} \sum_{p=1}^P \int_{S_p} J_z(\mathbf{r}') \int_0^\infty \left(\frac{e^{-\gamma_0|y-y'|} - e^{-\gamma_0(y+y')}}{2\gamma_0} + \frac{e^{-\gamma_0(y+y')}}{\gamma+\gamma_0} \right) \times \cos[\alpha(x-x')] d\alpha dS' \begin{pmatrix} y > 0 \\ y < 0 \end{pmatrix} \quad (2)$$

where $\mathbf{r}' = \mathbf{i}_x x' + \mathbf{i}_y y'$, $dS' = dx' dy'$, $\gamma_0^2 = \alpha^2 - \beta_0^2$, $\gamma^2 = \alpha^2 - \beta^2$, and the symbol α is the spectral parameter in the x direction. The unprimed symbols such as \mathbf{r} , x , and y concern the observation points, whereas the primed symbols such as \mathbf{r}' , x' , y' , and dS' are related with the source points. Expression (2) is subject to the condition of closed current that

$$\sum_{p=1}^P I_p = 0, \quad I_p = \int_{S_p} J_z(\mathbf{r}) dS \quad (3)$$

where I_p is the total current which flows in the p -th line. This condition has been often employed in deriving integral equations for multiconductor lines [8, 15] in order to keep the vector potential unique. In treating a single line, however, the formulation should be slightly modified as was done in our previous work (See Eq. (4) of [13]).

Let us deform (2) for $y > 0$ with paying attention to the denominators $2\gamma_0$ and $\gamma + \gamma_0$ in the integrand. The spectral integral concerning the first fraction including $2\gamma_0$ is evaluated with the aid of the integral representation of the Hankel function

$$H_0^{(2)}\left(\beta_0 \sqrt{x^2 + y^2}\right) = \frac{2j}{\pi} \int_0^\infty \frac{e^{-\gamma_0|y|}}{\gamma_0} \cos(\alpha x) d\alpha \quad (4)$$

We introduce the quasi-static approximation by assuming that the extent of the lines $Pw + (P - 1)s$ is much smaller than the vacuum wavelength $2\pi/\beta_0$. For example, if the maximum frequency is 10 GHz and the corresponding wavelength is 30 mm, lines having 1 mm-span is permissible. In this case, the variable of the Hankel function in (4) does not exceed $(2\pi/30 \text{ mm}) \times 1 \text{ mm} \approx 0.2$, which allows us to employ $H_0^{(2)}(\beta_0 r) \approx (-2j/\pi) \log r + \text{constant}$. Application of $\gamma_0 = (\alpha^2 - \beta_0^2)^{1/2} \approx \alpha[1 - (\beta_0/\alpha)^2/2] \approx \alpha$ ($\beta_0 \ll \alpha$) to the second fraction in the integrand of (2), we have

$$A_z(\mathbf{r}) = -\frac{\mu_0}{2\pi} \sum_{p=1}^P \int_{S_p} J_z(\mathbf{r}') \left[\log \left| \frac{\mathbf{r} - \mathbf{r}'}{\mathbf{r} - \bar{\mathbf{r}}'} \right| + L(\beta(\mathbf{r} - \bar{\mathbf{r}}')) \right] dS' \quad (y > 0) \quad (5)$$

where $\bar{\mathbf{r}}' = \mathbf{i}_x x' - \mathbf{i}_y y'$ denotes the image point of \mathbf{r}' with respect to the substrate surface $y = 0$. The logarithmic part of the kernel

corresponds to the case where the substrate is replaced by perfect conductor, whereas the function

$$L(\mathbf{i}_x\xi + \mathbf{i}_y\eta) = \frac{2}{\eta^2} \int_0^\infty [(\alpha^2 - \eta^2)^{1/2} - \alpha] \cos \frac{\alpha\xi}{\eta} e^{-\alpha} d\alpha \quad (6)$$

stands for a correction when its conductivity turns to finite value [16]. It is analytically evaluated by using the formula [17]

$$\int_0^\infty (\alpha^2 + \xi^2)^{1/2} e^{-\eta\alpha} d\alpha = \frac{\pi\xi}{2\eta} [\mathbf{H}_1(\xi\eta) - Y_1(\xi\eta)] \quad (7)$$

and its special case $\int_0^\infty \alpha e^{-\alpha} d\alpha = 1$ as $\xi \rightarrow 0$, where \mathbf{H}_1 and Y_1 are the Struve function and Neumann function, respectively. As a result we have

$$L(\mathbf{i}_x\xi + \mathbf{i}_y\eta) = \frac{\pi}{2} \left[\frac{\mathbf{H}_1(-\xi + j\eta) - Y_1(-\xi + j\eta)}{\xi - j\eta} - \frac{\mathbf{H}_1(\xi + j\eta) - Y_1(\xi + j\eta)}{\xi + j\eta} \right] + \frac{2(\xi^2 - \eta^2)}{(\xi^2 + \eta^2)^2} \quad (8)$$

2.3. Integral Equations

Employing the relations concerning the electric field that $\mathbf{E} = -j\omega\mathbf{A} - \nabla\phi = \mathbf{J}/\sigma$, with ϕ being a scalar potential, we are led to the set of integral equations for the current density as

$$J_z(\mathbf{r}) - \frac{j}{\pi\delta^2} \sum_{p'=1}^P \int_{S_{p'}} J_z(\mathbf{r}') \left[\log \left| \frac{\mathbf{r} - \mathbf{r}'}{\mathbf{r} - \bar{\mathbf{r}}'} \right| + L(\beta(\mathbf{r} - \bar{\mathbf{r}}')) \right] dS' = J_p^{ex} \quad (\mathbf{r} \in S_p; p = 1, 2, \dots, P) \quad (9)$$

where $\delta = \sqrt{2/(\omega\mu_0\sigma)}$ is the skin depth of the metal, and $J_p^{ex} = -\sigma(\partial\phi/\partial z)_{S_p}$ denotes the excitation current density. Note that, if the substrate is removed, (9) is reduced to the conventional form where the kernel is only $\log|\mathbf{r} - \mathbf{r}'|$ [5, 8, 9, 13]. This is understood by the fact that the small argument approximation $L(\mathbf{i}_x\xi + \mathbf{i}_y\eta) \approx \log\sqrt{\xi^2 + \eta^2} + constant$ cancels the image kernel $\log|\mathbf{r} - \bar{\mathbf{r}}'|$.

2.4. Method of Moments

Let us discretize (9) by the method of moments [14], where two-dimensional rectangular pulses are used for both basis and weighting functions [5, 9, 13]. We divide the cross section S_p into M and N segments in the x and y directions, respectively, as was done in

the present authors' recent work [13] which takes the skin effect into account. Then we may write as $S_p = \bigcup_{m=1}^M \bigcup_{n=1}^N S_{pmn}$. In the subsection S_{pmn} which has the area $\Delta S_{mn} = \Delta w_m \Delta t_n$, we approximate the current density $J_z(\mathbf{r})$ by a constant J_{pmn} . The procedure of taking moments leads us to the linear relations

$$J_{pmn} + \sum_{p'=1}^P \sum_{m'=1}^M \sum_{n'=1}^N G_{pmn,p'm'n'} J_{p'm'n'} = J_p^{ex}$$

$$(p = 1, 2, \dots, P; m = 1, 2, \dots, M; n = 1, 2, \dots, N) \quad (10)$$

where the operator element is arranged in the form of

$$G_{pmn,p'm'n'} = \frac{\Delta S_{m'n'}}{j\pi\delta^2} \left(\log \frac{R_{pmn,p'm'n'}}{\bar{R}_{pmn,p'm'n'}} + \bar{L}_{pmn,p'm'n'} \right) \quad (11)$$

The symbol $R_{pmn,p'm'n'}$ ($\bar{R}_{pmn,p'm'n'}$) denotes the geometrical mean distance between S_{pmn} and $S_{p'm'n'}$ (the image of $S_{p'm'n'}$) defined by

$$\log \left(\frac{R_{pmn,p'm'n'}}{\bar{R}_{pmn,p'm'n'}} \right) = \frac{\int_{S_{pmn}} \int_{S_{p'm'n'}} \log \left(\frac{|\mathbf{r} - \mathbf{r}'|}{|\mathbf{r} - \bar{\mathbf{r}}'|} \right) dS' dS}{\Delta S_{mn} \Delta S_{m'n'}} \quad (12)$$

with its analytical expression given in [9, 18]. The remaining part of (11), related to the function L , is simply approximated with sufficient accuracy as

$$\bar{L}_{pmn,p'm'n'} = \frac{\int_{S_{pmn}} \int_{S_{p'm'n'}} L(\beta(\mathbf{r} - \bar{\mathbf{r}}')) dS' dS}{\Delta S_{mn} \Delta S_{m'n'}}$$

$$\approx L \left(\beta \bar{R}_{pmn,p'm'n'} \frac{\mathbf{r}_{pmn} - \bar{\mathbf{r}}_{p'm'n'}}{|\mathbf{r}_{pmn} - \bar{\mathbf{r}}_{p'm'n'}|} \right) \quad (13)$$

where $\mathbf{r}_{pmn} = \mathbf{i}_x x_{pm} + \mathbf{i}_y y_{pn}$ ($\bar{\mathbf{r}}_{pmn} = \mathbf{i}_x x_{pm} - \mathbf{i}_y y_{pn}$) is the center of S_{pmn} (the image of S_{pmn}). Note that, although y_{pn} is independent of p in the case of horizontal arrangement like Fig. 1, we stand on this representation to retain generality.

Since the constants J_p^{ex} in (10) are also unknown, P conditions are lacking. These are supplemented by discretizing (3) as

$$\sum_{m=1}^M \sum_{n=1}^N J_{pmn} \Delta S_{mn} = I_p \quad (p = 1, 2, \dots, P) \quad (14)$$

where the constants I_p are preset. The set of Eqs. (10) and (14) are simultaneously solved for the $P(MN + 1)$ unknowns J_{pmn} and J_p^{ex} .

2.5. Impedance

Using the energy relations, we can write the per-unit-length resistance and internal inductance of the p -th line as

$$R_p = \frac{1}{\sigma |I_p|^2} \int_{S_p} |\mathbf{J}(\mathbf{r})|^2 dS \approx \frac{1}{\sigma |I_p|^2} \sum_{m=1}^M \sum_{n=1}^N |J_{pmn}|^2 \Delta S_{mn} \quad (15)$$

$$L_p^{in} = \frac{\mu_0}{|I_p|^2} \int_{S_p} |\mathbf{H}(\mathbf{r})|^2 dS \approx \frac{\mu_0}{|I_p|^2} \sum_{m=1}^M \sum_{n=1}^N |\mathbf{H}(\mathbf{r}_{pmn})|^2 \Delta S_{mn} \quad (16)$$

The magnetic field in (16) is computed from $\mathbf{H}(\mathbf{r}) = (1/\mu_0)\nabla \times \mathbf{A}(\mathbf{r})$ in the same way as [13].

Let the q -th ($q \neq P$) and P -th lines carry a loop current, i.e., $I_P = -I_q$ and $I_\ell = 0$ for all ℓ but q and P . After finding the set of J_ℓ^{ex} ($\ell = 1, 2, \dots, P$) under this situation, we can derive the per-unit-length resistance R_{pq} and inductance L_{pq} for an arbitrary pair of p and q (not including P) by equating the real and imaginary parts of the both sides of the relation [8, 15]

$$Z_{pq} = R_{pq} + j\omega L_{pq} = \frac{J_p^{ex} - J_P^{ex}}{\sigma I_q} \quad (p, q \neq P) \quad (17)$$

The cases $p = q$ and $p \neq q$ correspond to self and mutual impedances, respectively. If the reference line is not the rightmost one in Fig. 1, the numbering of lines should be altered so that the current returns through S_P .

In the special case of round-trip two-conductor lines, we can derive R_{11} and L_{11} from (17) at $P = 2$. By taking symmetry of the structure into account, the round-trip resistance and the external inductance are written as

$$R_1 + R_2 = 2R_1, \quad L^{ex} = L_{11} - L_1^{in} - L_2^{in} = L_{11} - 2L_1^{in} \quad (18)$$

Note that the difference $R_{11} - 2R_1$ is ascribed to the eddy current loss in the substrate. Then we have $R_{11} = 2R_1$ for free-standing lines.

3. NUMERICAL RESULTS

3.1. Free-Standing Lines

Let us treat some transmission lines without a substrate at first. Fig. 2 shows the frequency dependence of the per-unit-length impedance for two-conductor lines. The width $w = 20 \mu\text{m}$ and the thickness $t = 6 \mu\text{m}$ are the same as those chosen in [20]. The resistance $2R_1$ increases (the internal inductance $2L_1^{in}$ and external inductances L^{ex} decrease)

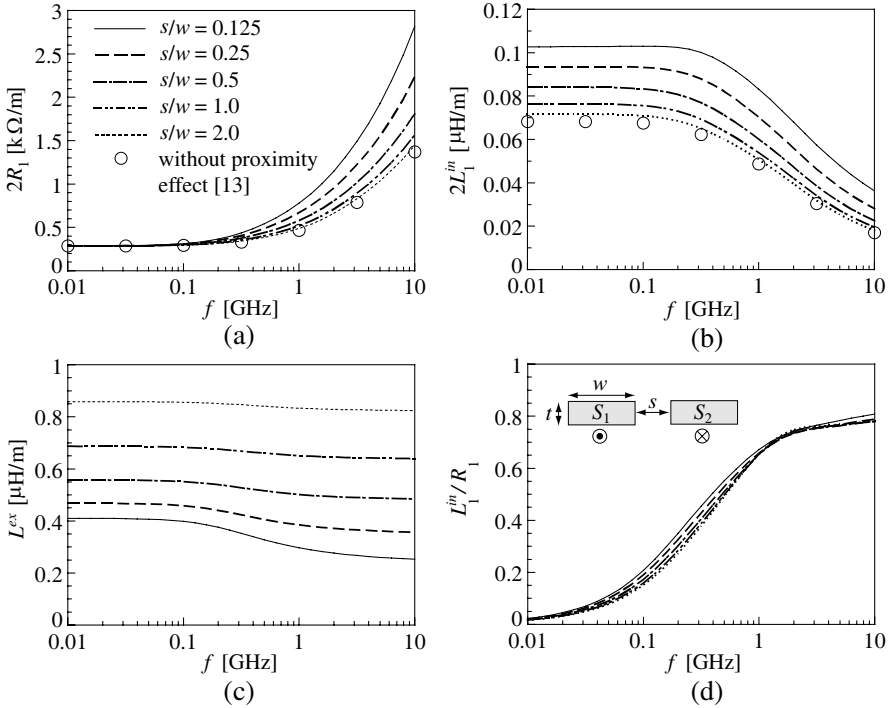


Figure 2. Frequency dependence of the per-unit-length impedance for two-conductor lines without a substrate. The parameters are $w = 20 \mu\text{m}$, $t = 6 \mu\text{m}$, and $\sigma = 58 \text{MS/m}$. Geometrical symmetry implies $R_1 = R_2$ and $L_1^{in} = L_2^{in}$. (a) Resistance. (b) Internal inductance. (c) External inductance. (d) Ratio of internal reactance to resistance.

monotonically with frequency f , which stems from the superposition of the skin and proximity effects. The latter effect, by which the current is shifted toward the facing sides, becomes prominent when the separation s is small. The behaviors of Figs. 2(a)–(c) are similar to those in Fig. 5 of [15] which was computed for the circular conductors. In Figs. 2(a), (b), the values of resistance and internal inductance without proximity effect are plotted by open circles. These are simply obtained by doubling the corresponding values for an isolated conductor [13]. The resistance $2R_1 = 2/(\sigma wt) = 287 \Omega/\text{m}$ is exact, whereas Eq. (30) of [19] can be used for the internal inductance, giving $2L_1^{in} = 68.6 \text{nH/m}$. The ratio of internal reactance to resistance is displayed in Fig. 2(d) to continue the discussions in [9, 13, 20, 21]. We see that the dependence of the ratio on s/w is weak at all frequencies.

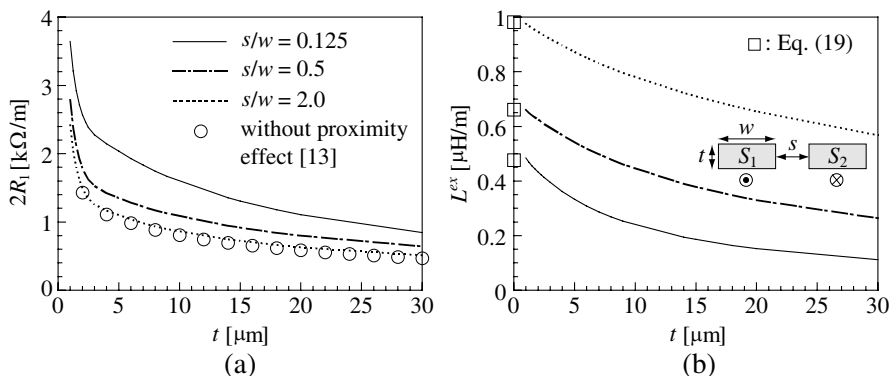


Figure 3. Thickness dependence of the per-unit-length impedance for two-conductor lines without a substrate. The parameters are $w = 20 \mu m$, $t = 6 \mu m$, $\sigma = 58 MS/m$, and $f = 5 GHz$. (a) Resistance. (b) External inductance.

This implies that the proximity effect, as well as the skin effect, acts on both resistance and internal inductance to a similar extent.

Figure 3 shows the thickness dependence of the per-unit-length impedance for two-conductor lines. The parameters are the same as those in Fig. 2, except that the frequency f is fixed at 5 GHz and the thickness t varies. Both the resistance $2R_1$ and external inductances L^{ex} are increased monotonically as t is decreased. The dependence on the distance s is similar to that of Figs. 2(a), (c). We notice the rapid growth in $2R_1$ when t goes under $2 \mu m$ that is comparable to the skin depth $\delta = 0.93 \mu m$. This is caused by the end effect of the knife edges. The external inductance for thin conductors approaches the analytical value based on the conformal mapping at zero thickness [22]

$$L^{ex} = \mu_0 \frac{K(\kappa)}{K(\sqrt{1 - \kappa^2})} \quad \left(\kappa = \frac{s/w}{2 + s/w}, t = 0 \right) \quad (19)$$

where $K(\cdot)$ is the complete elliptic integral of the first kind.

Figure 4 shows the characteristics of three-conductor lines, the center of which is the reference S_3 . Symmetry of the structure permits us to solve the problem only for $(I_1, I_3, I_2) = (1, -1, 0)$, resulting in $Z_{pq} = Z_{qp}$. The self resistance R_{pp} and the self-inductance L_{pp} agree well with $2R_1$ and $L^{ex} + 2L_1^{in}$ in Fig. 2. On the other hand, at $s/w = 2.0$ (dotted curve) and $f = 10 GHz$ for example, the mutual resistance R_{12} ($= R_{21}$) is about half of the self-resistance R_{11} ($= R_{22}$). A similar property is seen for the relation between the mutual inductance L_{12}

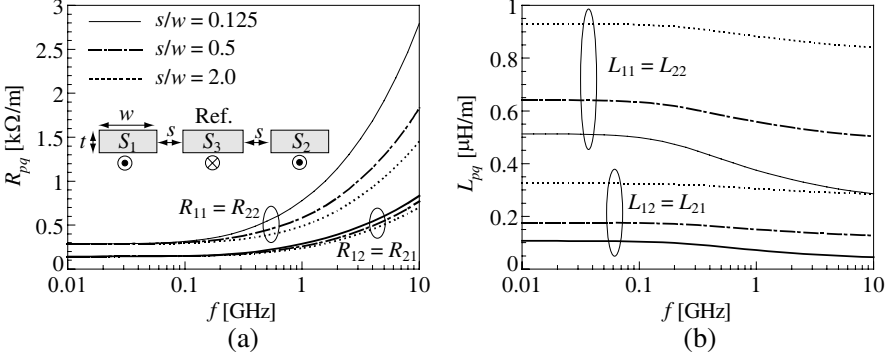


Figure 4. Frequency dependence of the per-unit-length impedance for three-conductor lines without a substrate. The parameters are $w = 20 \mu\text{m}$, $t = 6 \mu\text{m}$, and $\sigma = 58 \text{ MS/m}$. (a) Resistance. (b) Inductance.

and the self-inductance L_{11} . This implies that the crosstalk cannot be neglected when the gap is very small. The behaviors of Fig. 4 are similar to those in Fig. 6 of [15] which was obtained for the circular conductors.

3.2. Lines with Substrate

Next we will treat some lines with a lossy substrate. The eddy current induced in the substrate affects the line impedance. This current is expressed as follows. Substitution of (2) into $\mathbf{J}(\mathbf{r}) = (j\omega\epsilon^s + \sigma^s)\mathbf{E}(\mathbf{r}) = (\beta^2/\mu_0)\mathbf{A}(\mathbf{r})$ gives us the current density in the substrate region as

$$J_z(x, y) = -\frac{1}{\pi} \sum_{p=1}^P \sum_{m=1}^M \sum_{n=1}^N J_{pmn} \Delta S_{mn} \int_0^\infty [(\alpha^2 - \beta^2)^{1/2} - \alpha] \times \cos[\alpha(x - x_{pm})] e^{(\alpha^2 - \beta^2)^{1/2} y - \alpha y_{pn}} d\alpha \quad (y < 0) \quad (20)$$

where we have applied $J_z(\mathbf{r})|_{\mathbf{r} \in S_{pmn}} \approx J_{pmn}$ and $\gamma_0 \approx \alpha$. Performing the change of variables $u = \alpha(y_{pn} - y)$ and extracting the decaying factor e^{-u} from the integrand in (20), we can evaluate the semi-infinite integral accurately by employing the Gauss-Laguerre quadrature formula [17]. In the limiting case where $y \rightarrow 0$, namely, on the substrate surface, (20) is reduced to

$$J_z(x, 0) \approx -\frac{\beta^2}{2\pi} \sum_{p=1}^P \sum_{m=1}^M \sum_{n=1}^N J_{pmn} \Delta S_{mn} L(\beta(\mathbf{i}_x x - \bar{\mathbf{r}}_{pmn})) \quad (21)$$

where the function L is defined by (6) and can be evaluated by (8).

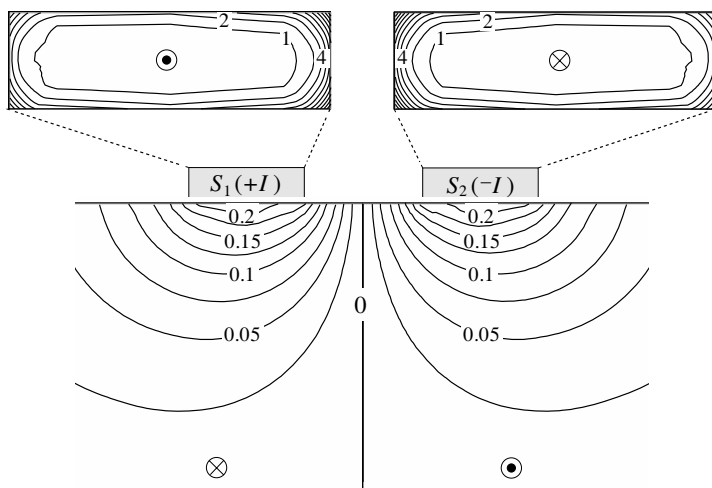


Figure 5. Normalized current density $|wtJ_z(x, y)/I|$ in the two line conductors and substrate. The parameters are $w = s = 20 \mu\text{m}$, $t = 6 \mu\text{m}$, $h = 0$, $\sigma = 58 \text{MS/m}$, $\epsilon^s = 12\epsilon_0$, $\sigma^s = 10 \text{kS/m}$, and $f = 5 \text{GHz}$.

Figure 5 shows the amplitude of current density in both the line conductors and substrate. The computational region of the substrate is $5w$ -width and $2.5w$ -depth. The contour map is odd symmetric with respect to the vertical line of symmetry. The value is normalized so that it would become unity in the DC limit, that is, we have the averaged current density $J_z(x, y) = \pm I/wt$ everywhere in the line conductors at $f = 0$, giving $|wtJ_z(x, y)/I| = 1$. For AC, the skin effect diminishes (boosts) the amount of current density in the central (surrounding) part of rectangles. At the present frequency as much as 5 GHz, the skin depth in the line conductors and substrate is $0.16t$ and $3.6w$, respectively. The latter is found from $1/\text{Re}\{[(j\omega\epsilon^s + \sigma^s)j\omega\mu_0]^{1/2}\}$. We observe the proximity effect of the two conductors as well as the concentration of eddy current toward the bottom of the metal lines.

The equivalent resistance due to the eddy current loss is written in the form of the integral over lower half plane as

$$R^{ed} = \frac{1}{\sigma^s |I|^2} \int_{-\infty}^{\infty} \int_{-\infty}^0 |\mathbf{J}(\mathbf{r})|^2 dy dx \tag{22}$$

where we have assumed that the line current has an identical amplitude $|I|$ for all conductors. Nevertheless, practical computations using (22) would be very time consuming. Alternatively, we express this

resistance by an integral of the Poynting power invading into the substrate as

$$R^{ed} = \text{Re} \left[-\frac{1}{|I|^2} \int_{-\infty}^{\infty} E_z(x, 0) H_x^*(x, 0) dx \right] \quad (23)$$

where the asterisk denotes complex conjugation. The above expression is deformed by the application of $E_z(\mathbf{r}) = -j\omega A_z(\mathbf{r})$ and $H_x(\mathbf{r}) = (1/\mu_0)(\partial A_z(\mathbf{r})/\partial y)$, and further, by the combination with the potential (2), the quasi-static approximation $\gamma_0 \approx \alpha$, and the relation

$$\begin{aligned} & \int_{-\infty}^{\infty} \cos[\alpha(x-x')] \cos[\alpha'(x-x'')] dx \\ &= \pi \cos[\alpha(x'-x'')] \left[\tilde{\delta}(\alpha+\alpha') + \tilde{\delta}(\alpha-\alpha') \right] \end{aligned} \quad (24)$$

with $\tilde{\delta}(\cdot)$ being the Dirac delta function. The result is compiled into

$$\begin{aligned} R^{ed} = \text{Re} & \left[\frac{j\omega\mu_0}{\pi|I|^2} \sum_{p=1}^P \int_{S_p} J_z(x', y') dx' dy' \sum_{p'=1}^P \int_{S_{p'}} J_z^*(x'', y'') dx'' dy'' \right. \\ & \left. \times F(\beta^* [\mathbf{i}_x(x'-x'') + \mathbf{i}_y(y'+y'')]) \right] \end{aligned} \quad (25)$$

where the change of variables $u = \alpha(y'+y'')$ gives

$$F(\mathbf{i}_x\xi + \mathbf{i}_y\eta) = \int_0^{\infty} \frac{(u^2 - \eta^2)^{1/2}}{|(u^2 - \eta^2)^{1/2} + u|^2} \cos \frac{\xi u}{\eta} e^{-u} du \quad (26)$$

This can be evaluated by the Gauss-Laguerre quadrature formula [17]. Discretization in terms of $J_z(\mathbf{r})|_{\mathbf{r} \in S_{pmn}} \approx J_{pmn}$ yields

$$\begin{aligned} R^{ed} = \text{Re} & \left[\frac{j\omega\mu_0}{\pi|I|^2} \sum_{p=1}^P \sum_{m=1}^M \sum_{n=1}^N J_{pmn} \Delta S_{mn} \sum_{p'=1}^P \sum_{m'=1}^M \sum_{n'=1}^N J_{p'm'n'}^* \Delta S_{m'n'} \right. \\ & \left. \times F \left(\beta^* \bar{R}_{pmn, p'm'n'} \frac{\mathbf{r}_{pmn} - \bar{\mathbf{r}}_{p'm'n'}}{|\mathbf{r}_{pmn} - \bar{\mathbf{r}}_{p'm'n'}|} \right) \right] \end{aligned} \quad (27)$$

in which the variable of function $F(\cdot)$ is the same as that of $L(\cdot)$ in (13) except that β is changed to β^* .

Figure 6 shows the frequency dependence of the per-unit-length impedance for two-conductor lines with a substrate. Total resistance R_{11} and the external inductance L_{11} are computed from (17) with $p = q = 1$ and $P = 2$. The conductivity σ^s can vary in wide range according to the doping rate for silicon [23], and we selected three

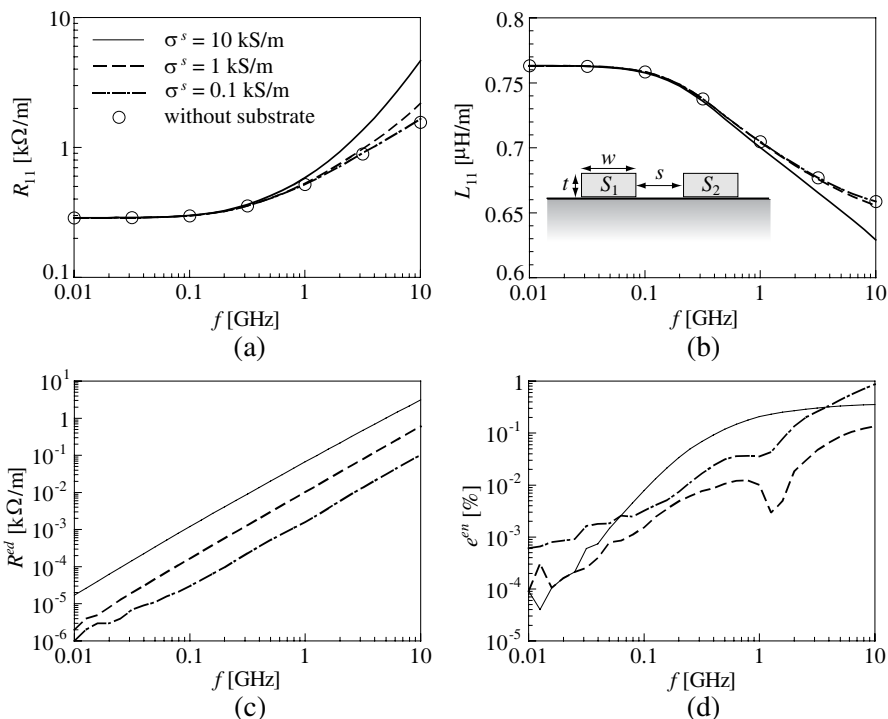


Figure 6. Frequency dependence of the per-unit-length impedance for two-conductor lines. The parameters are $w = s = 20 \mu\text{m}$, $t = 6 \mu\text{m}$, $h = 0$, $\sigma = 58 \text{ MS/m}$, and $\epsilon^s = 12\epsilon_0$. (a) Total resistance. (b) External inductance. (c) Resistance due to the eddy current loss. (d) Error based on the energy conservation.

practical values ranging from 0.1 kS/m to 10 kS/m. As seen from Figs. 6(a), (b), the increase in σ^s boosts the resistance (diminishes the inductance) compared with the free-standing case plotted by open circles. This situation stems out of the shift of eddy current toward the substrate surface, which is remarkable especially when the frequency increases. Fig. 6(c) is devoted to give the contribution of eddy current to resistance computed from (27). Seeing that the three curves exhibit rough linearity and equidistance, we can tell that R^{ed} is approximately proportional to $f^{1.5}$ and $(\sigma^s)^{0.7}$. Furthermore, it is important to mention that the law of energy conservation predicts the relation $R_{11} = 2R_1^{in} + R^{ed}$. Figs. 6(a) and 6(c) reveal that $R_{11} - R^{ed} (= 2R_1^{in})$ cannot be neglected, which is contrary to [10] mentioning that the skin effect in the interconnected conductors plays only a minor role.

Fig. 6(d) shows the computational error defined by

$$e^{en} = 2 \frac{R_{11} - 2R_1^{in} - R^{ed}}{R_{11} + 2R_1^{in} + R^{ed}} \times 100\% \quad (28)$$

where the internal resistance R_1^{in} is independently computed from (15). The error is always less than 1% under the condition that $M = 31$ (N changes from $(t/w)M$ to M according to f . See Section 3.2 of [13]) and that the number of the Gauss-Laguerre nodes for (26) is $2^9 = 512$. This result is satisfactory when considering that we have employed the quasi-static approximation in the derivation of (5).

Figure 7 shows the impedance of four-conductor lines as a function of the layer thickness h . The direction of current has odd symmetry such that $I_1 = I_2 = -I_3 = -I_4$, from which we can regard the geometry as a simplified model of the cross section of a flat spiral coil with two turns. In this case, the definition of the impedance (17) should be modified to

$$\left. \begin{aligned} Z_{p1} &= 2J_p^{ex}/(\sigma I) \Big|_{(I_1, I_2, I_3, I_4) = (I, 0, 0, -I)} \\ Z_{p2} &= 2J_p^{ex}/(\sigma I) \Big|_{(I_1, I_2, I_3, I_4) = (0, I, -I, 0)} \end{aligned} \right\} \quad (p = 1, 2) \quad (29)$$

The increase in h weakens the effect of the substrate, which brings low resistance and high inductance. In Fig. 7(a) the self resistance R_{11} is higher than R_{22} , because the eddy current loss due to the outer current loop S_1 and S_4 is greater than that by the inner conductors S_2 and S_3 . The mutual resistance $R_{21} = R_{12}$ is lower than the self ones similarly

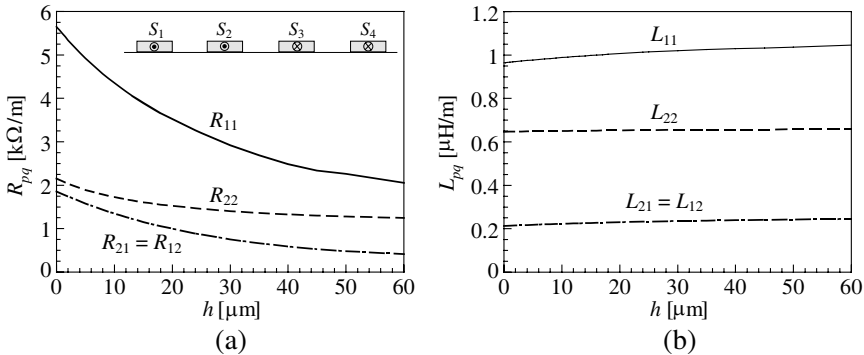


Figure 7. Height dependence of the per-unit-length impedance for four-conductor lines. The parameters are $w = s = 20 \mu\text{m}$, $t = 6 \mu\text{m}$, $\sigma = 58 \text{ MS/m}$, $\varepsilon^s = 12\varepsilon_0$, $\sigma^s = 10 \text{ kS/m}$, and $f = 5 \text{ GHz}$. (a) Resistance. (b) Inductance.

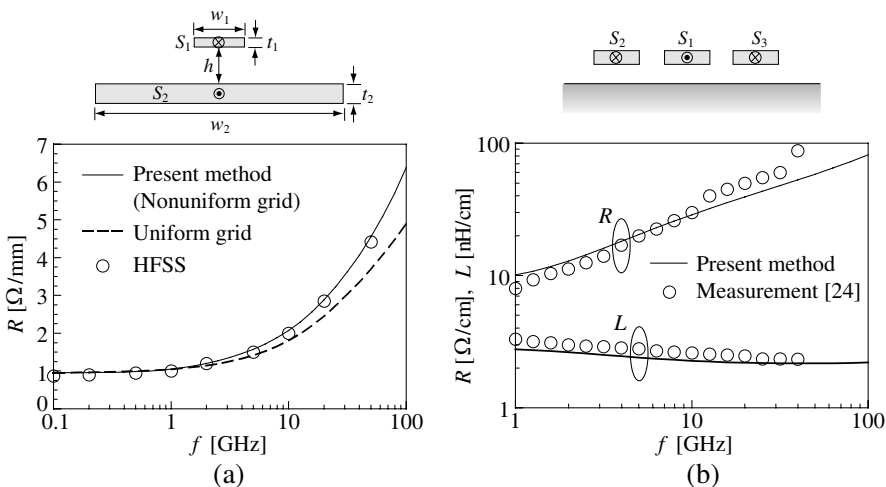


Figure 8. Numerical and experimental validation. (a) Comparison with Ansoft high frequency structure simulator. The parameters are $w_1 = w_2/5 = 10 \mu\text{m}$, $t_1 = t_2/2 = 2 \mu\text{m}$, $h = 8 \mu\text{m}$, and $\sigma = 58 \text{MS/m}$. (b) Comparison with measured data. The parameters are $w = 100t = 60 \mu\text{m}$, $s = 4 \mu\text{m}$, $h = 1.45 \mu\text{m}$, $\sigma = 33.3 \text{MS/m}$, $\epsilon^s = 12\epsilon_0$, and $\sigma^s = 8.70 \text{S/m}$.

to Fig. 4(a). This correspondence of self and mutual values also applies to the inductance L_{pq} in Fig. 7(b).

Figure 8 is devoted to the validation from the numerical and experimental viewpoints. The geometry of Fig. 8(a) is generalized from Fig. 1 so that the second conductor is regarded as a ground of microstrip line. The plotted values are the sum of the resistance for all conductors. We observe good agreement between the present solution and that by Ansoft HFSS. The dotted curve, which is obtained by using the uniform grid to discretize the cross section, is less accurate. Superiority of making the grid nonuniform according to the skin effect has also been demonstrated in Fig. 3 of [13]. Note that the number of division $M = 25$ is common to the two types of grids. On the other hand, Fig. 8(b) compares with the experimental data for a coplanar line presented in Fig. 6(a) of [24]. In principle, we need to consider two kinds of current loops that $(I_1, I_2, I_3) = (1/2, -1/2, 0)$ and $(1/2, 0, -1/2)$. Nevertheless, the symmetry allows us to solve only the case of $(I_1, I_2, I_3) = (1, -1, 0)$. The resistance of only the signal line S_1 is plotted. Though the structures treated by the computation and experiment are not necessarily identical with respect to the width

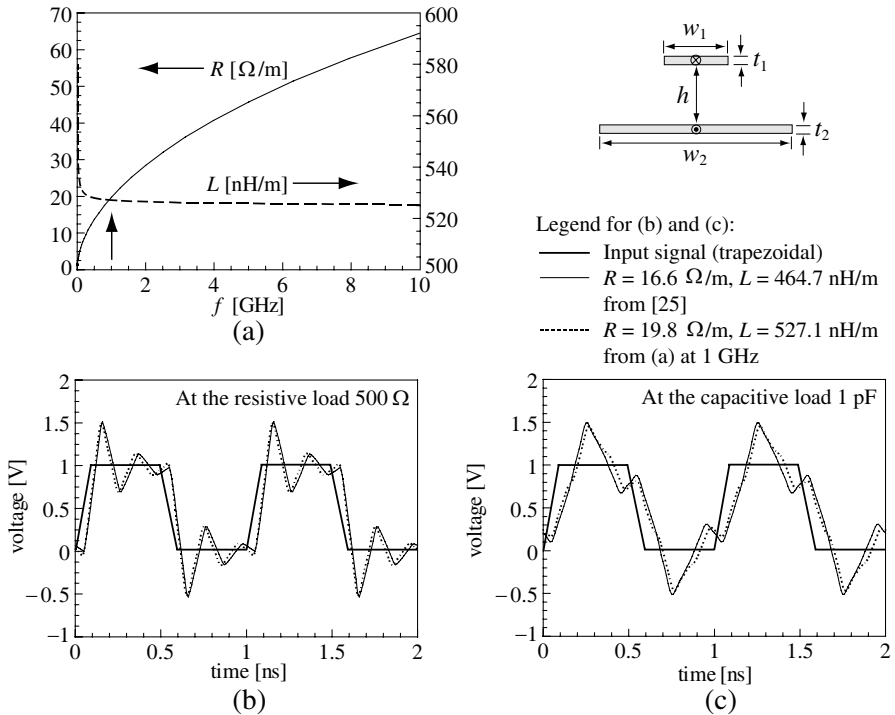


Figure 9. Computational results for the microstrip structure. The parameters are $w_1 = w_2/3 = 500 \mu\text{m}$, $t = 35 \mu\text{m}$, $h = 625 \mu\text{m}$, and $\sigma = 57 \text{MS/m}$. (a) Present numerical solution. (b), (c) Time responses at the resistive or capacitive load. The parameters common to [25] are the per-unit-length values $C = 74.7 \text{pF/m}$ and $G = 5.6 \text{mS/m}$, the line length = 8.5 mm, and the source impedance = 10 Ω .

of outer conductors and the thickness of substrate, this comparison is worth doing. In fact, the agreement in Fig. 8(b) is better than that of Fig. 6(a) in [24] where the comparison with RLGC transmission line model is shown.

Figure 9 is presented as the start of considering signal integrity. As shown in Fig. 9(a), the per-unit-length parameters R and L for the microstrip structure are computed in the same way as in Fig. 8(a). By supplement of the remaining parameters C and G , the transmission line forms a distributed circuit. Connecting the source and load to this line of finite length, we can observe the time response as shown in Figs. 9(b), (c). The input signal has a trapezoidal form, where the period is 1 ns (the fundamental frequency is 1 GHz), the rise time and

fall time are both 0.1 ns, the duration time is 0.4 ns, and the low (high) voltage is 0 V (1 V). We followed [25] as to the values of C and G , the line length, and the input parameters. The solid curves are obtained by using the values of R and L given in [25], whereas the dotted ones stand on the data in Fig. 9(a) at 1 GHz. The curves are close with each other, and also have similar shapes presented in Figs. 7 and 8 of [25]. Note that the time responses in Figs. 9(b), (c) are obtained in the analytical way on the circuit theory; we first compute the Fourier coefficient of the input as well as the system function of the transmission line at each frequency of harmonics, and then take the linear combination of them.

4. CONCLUSION

The numerical solution has been developed to compute the per-unit-length impedances of rectangular transmission lines backed by semi-infinite lossy substrate. The problem is formulated into a set of integral equations, the kernel of which is analytically expressed in terms of special functions in the quasi-static regime. This set is numerically solved by means of the method of moments. The numerical computations are carried out for some types of parallel lines, composed of two, three, and four conductors, by changing several line parameters. It has been shown that, due to the influence of eddy current in the substrate, the resistance and external inductance at high frequencies become emphasized. This implies that the substrate loss cannot be neglected. The correctness of the method is demonstrated by showing that the computed values of resistance satisfy the law of energy conservation with acceptable accuracy.

Though the present formulation takes into account only the axial component of the electric field or current density, it will become important to include the radial component when the lines operate at even higher frequencies [26, 27]. In fact, the numerical example in [26] shows that the mode supported by the conductor with a 2 mm-span begins to deviate from TEM one even at 1 GHz. If the conductor size is reduced to $632 \mu\text{m}$ ($= 2 \text{ mm}/\sqrt{10}$), the corresponding frequency is 10 GHz which is the highest one considered in the present paper. This problem deserves further attention.

REFERENCES

1. Hall, S. H. and H. L. Heck, *Advanced Signal Integrity for High-Speed Digital Designs*, John Wiley & Sons, 2009.

2. Bogatin, E., *Signal and Power Integrity — Simplified*, Pearson Education, 2009.
3. Cockcroft, J. D., “Skin effect in rectangular conductors at high frequencies,” *Proc. Roy. Soc. London*, Vol. A122, 533–542, 1929.
4. Smith, G. R., “Proximity effect in systems of parallel conductors,” *J. Appl. Phys.*, Vol. 43, No. 5, 2196–2203, 1972.
5. Berleze, S. L. M. and R. Robert, “Skin and proximity effects in nonmagnetic conductors,” *IEEE Trans. on Education*, Vol. 46, No. 3, 368–372, 2003.
6. Faraji-Dana, R. and Y. Chow, “Edge condition of the field and a.c. resistance of a rectangular strip conductor,” *IEE Proc.*, Vol. 137, Pt. H, No. 2, 133–140, 1990.
7. Kiang, J.-F., “Integral equation solution to the skin effect problem in conductor strip of finite thickness,” *IEEE Trans. on Microwave Theory and Tech.*, Vol. 39, No. 3, 452–460, 1991.
8. Sarkar T. K. and A. R. Djordjević, “Wideband electromagnetic analysis of finite-conductivity cylinders,” *Progress In Electromagnetics Research*, Vol. 16, 153–173, 1997.
9. Antonini, G., A. Orlandi, and C. R. Paul, “Internal impedance of conductors of rectangular cross section,” *IEEE Trans. on Microwave Theory and Tech.*, Vol. 47, No. 7, 979–985, 1999.
10. Ymeri, H., B. Nauwelaers, and B. Maex, “Distributed inductance and resistance per-unit-length formulas for VLSI interconnects on silicon substrate,” *Microwave and Optical Technology Letters*, Vol. 30, No. 5, 302–304, 2001.
11. Niknejad, A. M. and R. G. Meyer, “Analysis of eddy-current losses over conductive substrates with applications to monolithic inductors and transformers,” *IEEE Trans. on Microwave Theory and Tech.*, Vol. 49, No. 1, 166–176, 2001.
12. Tsuchiya, A. and H. Onodera, “Patterned floating dummy fill for on-chip spiral inductor considering the effect of dummy fill,” *IEEE Trans. on Microwave Theory and Tech.*, Vol. 56, No. 12, 3217–3222, 2008.
13. Matsuki, M. and A. Matsushima, “Improved numerical method for computing internal impedance of a rectangular conductor and discussions of its high frequency behavior,” *Progress In Electromagnetics Research M*, Vol. 23, 139–152, 2012.
14. Harrington, R. F., *Field Computation by Moment Methods*, Macmillan, New York, 1968.
15. Matsushima, A. and H. Sakamoto, “Application of wire model to calculation of impedance of transmission lines with arbitrary

- cross sections,” *Electronics and Communication in Japan (Part II: Electronics)*, Vol. 85, No. 7, 1–10, 2002.
16. Carson, J. R., “Wave propagation in overhead wires with ground return,” *Bell Sys. Tech. J.*, Vol. 5, 539–554, 1926.
 17. Abramowitz M. and A. Stegun, *Handbook of Mathematical Functions*, Ch. 12, Dover, New York, 1972.
 18. Higgins, T. J., “Formulas for the geometrical mean distance of rectangular areas and line segments,” *Appl. Phys.*, Vol. 14, No. 2, 188–195, 1943.
 19. Holloway, C. L. and E. F. Kuester, “DC internal inductance for a conductor of rectangular cross section,” *IEEE Trans. on Electromag. Compat.*, Vol. 51, No. 2, 338–344, 2009.
 20. Heinrich, W., “Comments on ‘Internal impedance of conductors of rectangular cross section’,” *IEEE Trans. on Microwave Theory and Tech.*, Vol. 49, No. 3, 580–581, 2001.
 21. Rong, A. and A. C. Cangellaris, “Note on the definition and calculation of the per-unit-length internal impedance of a uniform conducting wire,” *IEEE Trans. on Electromag. Compat.*, Vol. 49, No. 3, 677–681, 2007.
 22. Ghione, G. and C. Naldi, “Analytical formulas for coplanar lines in hybrid and monolithic MICs,” *Electron. Lett.*, Vol. 20, No. 4, 179–181, 1984.
 23. Hasegawa H., M. Furukawa, and H. Yanai, “Properties of microstrip line on Si-SiO₂ system,” *IEEE Trans. on Microwave Theory and Tech.*, Vol. 19, No. 11, 869–881, 1971.
 24. Milanović, V., M. Olgur, D. C. DeGroot, J. A. Jargon, M. Gaitan, and M. E. Zaghoul, “Characterization of broad-band transmission for coplanar waveguides on CMOS silicon substrates,” *IEEE Trans. on Microwave Theory and Tech.*, Vol. 46, No. 5, 632–640, 1998.
 25. Eudes T., B. Ravelo, and M. Louis, “Transient response characterization of the high-speed interconnection RLCG-model for the signal integrity analysis,” *Progress In Electromagnetics Research*, Vol. 112, 183–197, 2011.
 26. Stratton, J. A., *Electromagnetic Theory*, Sec. 9.16, McGraw-Hill, NY, 1941.
 27. Ilarionov, Y. A., E. A. Bukvarev, I. D. Krotov, and V. I. Naryshkin, “The fundamental electromagnetic wave of a single-wire line in a weakly absorbing medium,” *J. Commun. Tech. Electron.*, Vol. 52, No. 2, 140–146, 2007.